Frontier Example in Experimental Charge Density Research: Experimental Electrostatics of Proteins

C. LECOMTE,[1] B. GUILLOT,[1] C. JELSCH,[1] A. PODJARNY[2]

[1]*LCM3B, CNRS, Faculté des Sciences et Techniques, Université Henri Poincaré, Nancy 1, BP 239, 54506 Vandoeuvre-lès-Nancy, France*

[2]*UPR de Biologie Structurale, IGBMC, 1 rue Laurent Fries, 67404 Illkirck, France*

Received 10 December 2003; accepted 30 April 2004
Published online 25 October 2004 in Wiley InterScience (www.interscience.wiley.com).
DOI 10.1002/qua.20317

ABSTRACT: The experimental charge density methodology is extended to macromolecular structure and biocrystallography. Ultrahigh-resolution diffraction data now can be collected at third-generation synchrotron sources for well-ordered protein crystals; the data can be refined with a more sophisticated model than the independent atom model (IAM), such as the multipolar atom. A new crystallographic program MoPro combining small molecules and macromolecular refinement method has been developed; first applications are described. Int J Quantum Chem 101: 624–634, 2005

Key words: protein crystallography; electron density; pharmacology; molecular modelling; protein–ligand interactions

Introduction

Electron density studies are now a very mature field in small molecule crystallography; it is one of the most efficient experimental methods to derive electronic structure of solids. This article shows how it can be extended to macromolecular structures. Since 1990, the amount of high- or ultra-high-resolution protein X-ray diffraction data has increased almost exponentially, as demonstrated in Protein Data Bank records and by recent reviews [1–5]. We have recently shown that these data ($d <$ 1 Å) deserve a more sophisticated model than the usual spherical free atom model, called the independent atom model (IAM), which does not take into account the charge transfer and deformation of the valence electron density resulting from chemical bonding and intermolecular interactions [4, 6–7]. Hence, at these atomic resolutions, the charge transfer and asphericity of the electron density can be quantified using a model developed in small molecule accurate crystallography: the multipole model [8, 9]. This multipole model, described in detail below, gives an analytical representation of

Correspondence to: C. Lecomte; e-mail: claude.lecomte@lcm3b.uhp-nancy.fr

the charge density that enables experimental estimation of the electrostatic properties: electrostatic potential, electric field, electrostatic interaction energy [10–15], as well as dipole and higher multipole moments [16].

As high-resolution crystallography allows precise location of the atoms in the active site, including hydrogen atoms, the resulting atomic model may also be used for first principles calculations using density functional theory (DFT). Recent DFT developments such as linear scaling, which scales linearly with the number of atoms of the system rather than with the cube [17, 18] allow quantum calculations for biological systems of about 1000 atoms. Such a procedure was first applied to the protein crambin with SIESTA software [18]. Therefore, both experimental and theoretical methods are now available for fine estimation of protein–ligand or protein–protein interactions. The following review describes the experimental X-ray method: the first section concerns the methods used, and the second gives applications to a scorpio toxin [6] and to an aldose reductase complex [4].

Part I: Methodology

In small molecule crystallography, experimental electron densities are obtained by analysis of single-crystal X-ray diffraction measured to $d \approx 0.5$ Å resolution.

$$d = \lambda / 2 \sin \theta = 0.5 \text{ Å} \tag{1}$$

where θ is the Bragg angle and λ is the wavelength. For protein crystals, very high resolution comes from highly ordered crystals with a small proportion of solvent. It implies low-temperature factors ($B < 8$ Å^2, where $B = 8\pi^2 \langle u^2 \rangle$, $\langle u^2 \rangle$ being the mean square atomic displacement around equilibrium position) in the protein part to be modelled by an aspherical atom model [19], which can be attained when the data resolution is smaller than 0.9 Å.

INDEPENDENT ATOM MODEL (IAM)

Single crystal X-ray diffraction data lead to structure factor amplitudes. The structure factors F of the reflections $\mathbf{H} = (h, k, l)$ are the Fourier transform of the electron density $\rho_{\text{dyn}}(\mathbf{r})$ of the unit cell of volume V and parameters $a_{i,\ i=1,\ 3}$.

$$F(\mathbf{H}) = \int_{\text{unit cell}} \rho_{\text{dyn}}(\mathbf{r}) \exp(2i\pi \mathbf{H} \cdot \mathbf{r}) d^3\mathbf{r}. \tag{2}$$

The electron density ρ_{dyn} in the unit cell, which is affected by the atomic thermal motion, is obtained by a summation of convolution products:

$$\rho_{\text{dyn}}(\mathbf{r}) = \sum_{\text{atoms}} \rho_{\text{at,static}} * P_{\text{at}}(\mathbf{r}) \tag{3}$$

where $\rho_{\text{at,static}}$ is the atomic electron density at rest, P_{at} is an atomic probability distribution function, and its Fourier transform is the Debye–Waller factor. The crystal is triply periodic; therefore, the Fourier transform has nonzero values only on reciprocal lattice points defined by the reciprocal vectors

$$\mathbf{a}_i^* = (\mathbf{a}_j \wedge \mathbf{a}_k) V^{-1} \tag{4}$$

$F(\mathbf{H})$ are complex quantities, and both amplitude and phase must be known to directly calculate $\rho_{\text{dyn}}(\mathbf{r})$ by inverse Fourier transform. Methods for ab initio phase determination are still under development but they are the aim of this article. As the electron density is mainly concentrated around atomic positions, the structure factor may be expressed as a sum over pseudoatoms in the unit cell:

$$F(\mathbf{H}) = \sum_j f_j(|\mathbf{H}|) \exp(2i\pi \mathbf{H} \cdot \mathbf{r}_j) \exp(-0.25 B_j |\mathbf{H}|^2) \tag{5}$$

where $|\mathbf{H}| = 2 \sin \theta / \lambda$, $\mathbf{r}_j$ is the atomic position of the jth atom, B_j are its isotropic Debye–Waller factors, and f_j its atomic scattering factor; the latter are the Fourier transform of the electron density of the free spherical neutral atom (IAM).

This is the basic equation for most macromolecular crystallographic refinements that fit the observed $|F|$ values using a model with four parameters per atom, i.e., atomic coordinates and isotropic Debye–Waller factor. At the usual resolution for macromolecular crystallography (2 Å $< d <$ 3 Å), the resolution, and therefore the number of observations $|F|$, is not enough to determine the total number of parameters, and it has to be completed with relations imposing a standard stereochemistry for the polypeptide chain. At higher resolution, one can observe deviations from the standard geometry. If the data are at atomic resolution ($d <$ 1.3 Å), the isotropic temperature factor may be replaced by

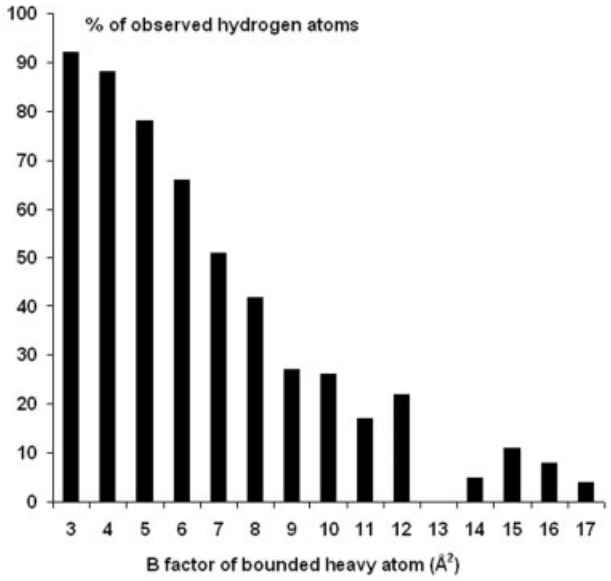

FIGURE 1. Percentage of the hydrogen atoms observed according to the equivalent *B* temperature factor of the bonded heavy atom in the structure of aldose reductase, refined at 0.66 Å resolution [20, 21].

an anisotropic factor, and the resulting accuracy of atomic positions is good enough to validate shifts from the standard geometry.

SUBATOMIC RESOLUTION AND CHARGE DENSITY MODELING

At subatomic resolution ($d < 0.9$ Å), information on valence electron density distribution may be obtained when the anisotropic displacement parameters (ADPs) are small. Hydrogen atoms also clearly show up. Deviations from the spherical atom model appear as electron density peaks in the bonds on deformation electron density maps (calculated by the difference between the observed electron density and the IAM density). For example, in the aldose reductase structure, 54% of hydrogen atoms were identified as well as most of the bonding density in the bonds of the active site of the protein [20, 21]. The probability of observing these features is directly related to the thermal displacement parameters or to the equivalent *B* factor [1–3] (Fig. 1).

CHARGE DENSITY REFINEMENT

The Multipolar Model and Derived Properties

The IAM model is too primitive to take into account all the information existing at subatomic resolution; so a new charge densities model derived from small molecule crystallography has been developed, called the multipolar model [8, 9, 22].

In contrast to the IAM model, where all atoms of a molecule or protein are supposed to be neutral with a spherical valence electron distribution (promolecule), the valence charge density is modeled by a sum of multipolar pseudoatoms lying at atomic positions. The valence electron density of such a pseudoatom is projected on the basis of real spherical harmonics functions y_{lm} centered on each pseudoatom:

$$\rho_{stat}(\mathbf{r}) = \rho_{core}(r) + \kappa^3 P_v \rho_{val}(\kappa \cdot r) + \sum_{l=0,1\ max} \kappa'^3 R_l(\kappa' \cdot r) \sum_{m=-1,1} P_{lm} y_{lm}(\theta, \varphi). \quad (6)$$

The radial functions $R_l(r)$ used here are of Slater type: $R_l(r) = r^{nl} \exp(-\kappa' \xi r)$. The first applications of this formalism to mono- or dipeptides has concerned the calibration of ab initio HF calculations: it was clearly shown that triple-ζ basis sets with polarization functions are necessary to quantitatively reproduce the X-ray diffraction experiment [23]. The charge density parameters P_v, P_{lm} (valence and multipolar populations, respectively) and κ, κ' (dilation and contraction of the spherical and nonspherical valence density, respectively) are directly obtained from least squares refinement against the structure factor amplitudes [8, 9, 22]. This analytical representation of the charge density is used to calculate crystal and molecular properties such as electrostatic potential [24], electric field, net charges, higher moments [16], and topology of the electron density [25]. As an example, Figure 2 shows the experimental electrostatic potential around $NADP^+$, which is the cofactor of numerous enzymatic oxydoreduction reactions. This potential was modeled from a high-resolution X-ray multipolar analysis of its analogue molecule NAD^+ (see Part II) [26]. The electropositive and electronegative regions around the molecule are clearly evidenced. The extended positive electrostatic potential generated by the C18 atom (Fig. 2) is in line with the ability of NAD^+ to accept in this position a negatively charged hydride ion during oxidation reactions.

The Multipolar Parameters Library

High resolution X-ray diffraction studies have been performed in Nancy on a large group of

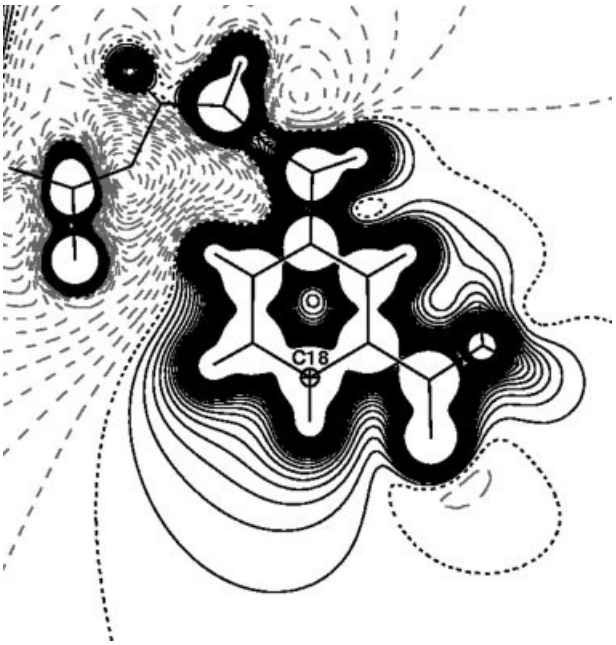

FIGURE 2. Electrostatic potential generated around the nicotinamide moiety of $NADP^+$ (calculated from subatomic resolution diffraction data). Contours, 0.05 $e\text{Å}^{-1}$; continuous black line, $\Phi > 0$; broken grey line, $\Phi < 0$; dotted black line, $\Phi = 0$ $e\text{Å}^{-1}$.

mono-, di-, or tri-peptides to determine precisely the electron density distribution of all natural aminoacids (see, e.g., Refs. [23, 27, 28]). These studies allowed building an experimental database of atomic charge density parameters (P_v, P_{lm}, κ, κ') [29] for each type of atom in a given chemical environment. These parameters were shown to be transferable to amino acids in proteins [30]. Figure 3 gives the static deformation electron density calculated from this multipolar parameters library for the CONH peptide group, as follows:

$$\delta\rho(\mathbf{r}) = \sum_{j=1,Nat} [\rho_{base}(\mathbf{r} - \mathbf{r}_j) - \rho_{promolecule}(\mathbf{r} - \mathbf{r}_j)].$$

This experiment-based deformation density reveals the valence electron redistribution due to covalent interactions. The electrons built up in the bonding region and the oxygen lone pairs clearly show up. Disposing of a reliable charge density library, the next step has been testing this database on a protein. X-ray diffraction data on crambin, which is a small 46 residues protein, have been measured on BW7A line of DORIS (Hamburg) synchrotron to a resolution of $d = 0.54$ Å by Teeter et al. [31], which is still the world record for a protein. This protein possesses the criterion for testing a charge density study (low Debye Waller factors: $B \sim 3$ $Å^2$ for ordered parts of the protein). Taking advantage of the repetition of the $CONHC_\alpha H_\alpha$ chemical motif along the polypeptide main chain, the average dynamic deformation map (Fig. 4) over the 34 nondisordered peptide residues was calculated according to

$$\delta\rho(\mathbf{r}) = \sum_{H'} (Fo - Fc)\exp(i\varphi_c)\exp(-2i\pi\mathbf{H}\cdot\mathbf{r}), \quad (7)$$

where Fc and φc are respectively the structure factor amplitude and the phase calculated according to the IAM model (neutral, spherical atoms). Fo is the structure factor amplitude derived from the synchrotron experiment. This average deformation density map displays significant residual density in the bonds between nonhydrogen atoms and on oxygen lone pairs at their expected positions and is similar to Figure 3. These features clearly demonstrate that the IAM model does not provide a fully adequate fit to the experimental diffraction data.

After transfer of the statistically significant multipoles from the database and after multipolar refinement (using MOLLY software [9]), the residual density does not exceed 0.06 $e\text{Å}^{-3}$, which is about the estimated error. The progressive flattening of

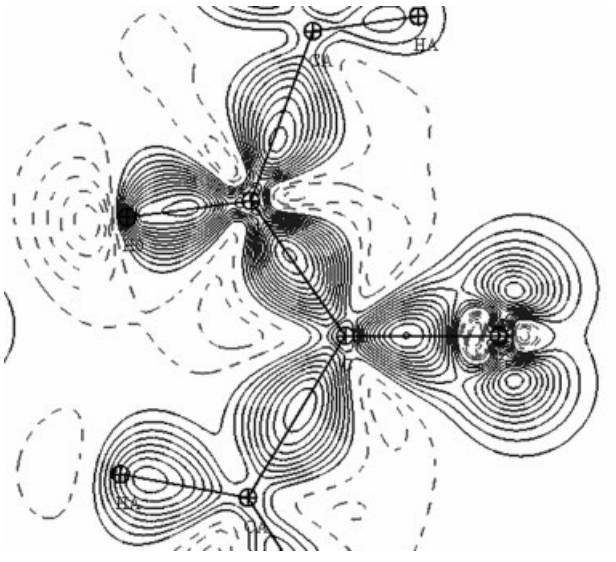

FIGURE 3. Deformation electron density in the peptide plane calculated from the multipolar database [29]. Contours, 0.05 $e\text{Å}^{-3}$; continuous lines, $\delta\rho > 0$; broken lines, $\delta\rho < 0$.

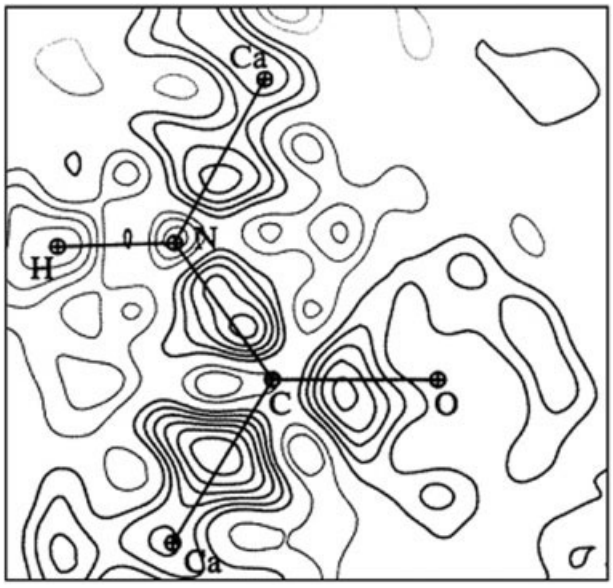

FIGURE 4. Residual electron density averaged over the 34 non-disordered peptide groups of crambin after an IAM modelling. Positive density in black contours and negative in grey.

residual density features through the refinement stages was a convincing physical evidence of real improvement in the modelling [7]. At the end of the refinement, the static deformation electron density of the average peptide residue (Fig. 5) is in almost quantitative agreement with that derived from a triple-ζ HF calculation on a single monopeptide [23].

The MoPro Refinement

As these results were very encouraging, a new software refinement program (MoPro) was written [22]; it combines the advantages of small-molecule multipolar refinement with anisotropic atom refinement of proteins and runs on scalar or parallel computers. To extract the aspherical features of the electron density, the following strategy was designed: first, a full anisotropic spherical atom refinement using starting parameters from a SHELXL [32] refinement is performed on all non-disordered atoms using (or not depending on the data quality and on the atomic *B* factors) bond lengths, angle, planarity, rigid bond [33] restraints using all diffraction data, whatever the resolution. Then, a subset of the structure based on equivalent *B* factors less than a given threshold (8–12 Å^2) is selected to perform the electron density analysis. At first, a high-order (HO) spherical atom refinement on the non-hydrogen atoms is performed to obtain the least-biased positional and thermal parameters.

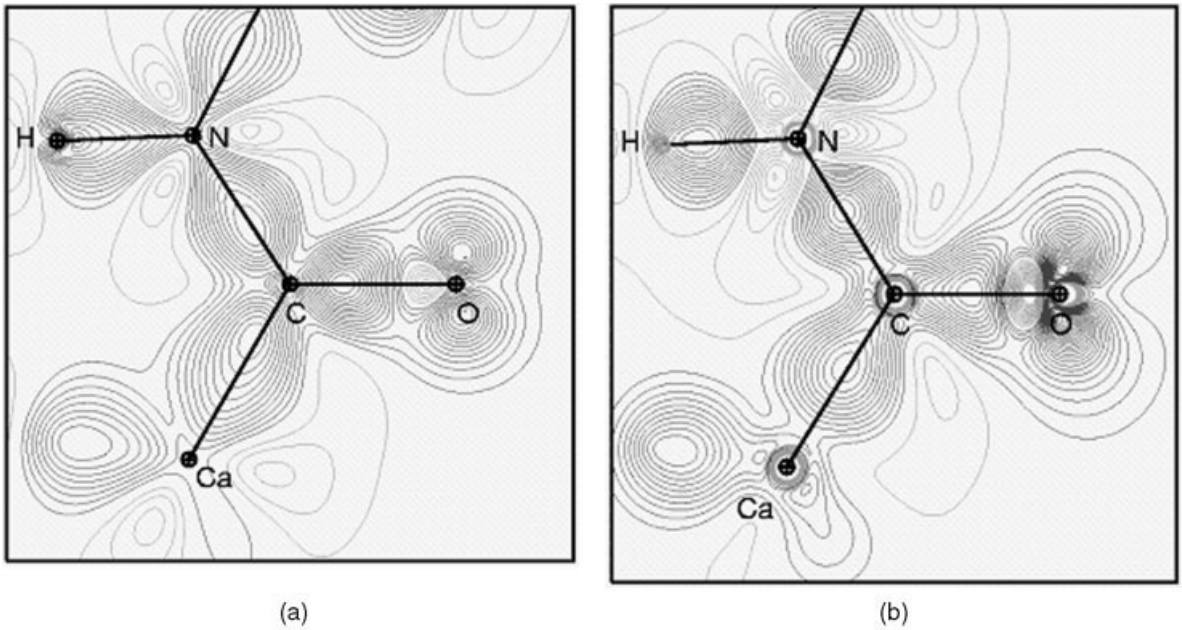

FIGURE 5. Static deformation density of a peptide plane in crambin (a), compared to a HF SCF calculation on a single peptide [23] (b). Contours positive in black and negative in grey.

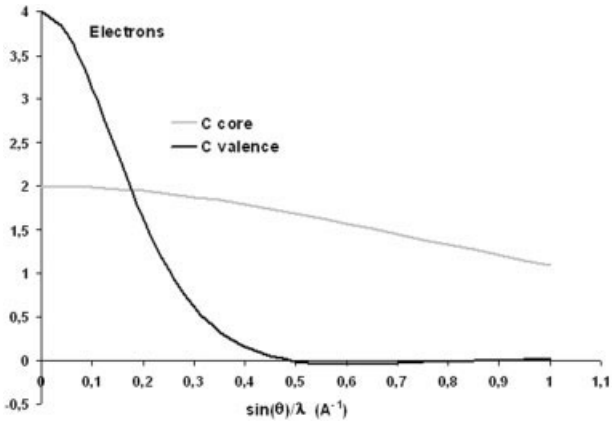

FIGURE 6. Atomic scattering factor for a hypothetical static carbon atom ($B = 0$ Å^2) as a function of reciprocal resolution sin θ/λ (Å^{-1}). Black line represents valence electrons, and dotted grey line for core electrons.

Figure 6 gives the carbon atomic scattering factor (f) as a function of resolution. The scattering factor is the Fourier transform of the atom electron density: because of the properties of the Fourier transform, this HO procedure refines the positional and anisotropic thermal motion parameters only against core electrons (Fig. 6). Because valence electron scattering factors diffuse only at low resolution, HO refinement gives precise positions and displacements of the core electrons only.

In the second stage of the refinement, the starting deformation valence density parameters of the atoms of the selected fragments are automatically transferred from our charge density parameter database [29] using a well-defined MoPro procedure. This means that all atoms of the selected fragment are charged atoms and are assigned nonspherical atomic scattering factors. All H atoms are then displaced along the X—H bonds to standard bond distances obtained from neutron studies. Usually, after few refinement cycles of X, Y, Z, and U_{ij} the transfer procedure leads to a large improvement of the refinement. Because a part of the nonspherical atom scattering density was taken into account, it also leads to more accurate positions and thermal motion parameters (see, e.g., the charge density analysis of NAD^+ in Ref. [26]). Then the charge density parameters, including H atoms, can be refined using or not using—depending on the data quality—electron density restraints or constraints (chemical equivalence, site symmetry) that are part of the MoPro algorithms.

At the end of the refinement, one obtains the best experimental description of the electron density, which can be used to compute the electrostatic potential [14]. This procedure was successfully applied to a human aldose reductase complex, for which ultrahigh-resolution data (0.66 Å) were collected [4, 20] on the ID19 beamline at the Advanced Photon Source synchrotron (APS–ANL, Argonne, IL) in collaboration with A. Joachimiak.

Part II: Some Examples

PROTEIN ELECTROSTATICS USING THE CHARGE DENSITY DATABASE

A first application of these methods is the calculation of electrostatic properties for proteins with X-ray data at atomic resolution (about $0.9 < d < 1.5$ Å). At these resolutions, the atomic positions in the active site, including H atoms, are usually clearly defined. Therefore a direct use of the charge density database [28] permits, using the MoPro software, a quick calculation of the electrostatic potential; the resulting potential was shown to compare very well with much more time consuming theoretical methods like DFT calculations [4]. This can now be almost routinely performed, at very low cost, after any spherical atom refinement. A successful application has been obtained with the 0.66 Å aldose reductase complex, although this resolution clearly allows an effective refinement of the transferred charge density parameters (see below).

As shown in Figure 7, the complex is made of the aldose reductase protein, the $NADP^+$ cofactor and an inhibitor. To precisely determine the interaction between $NADP^+$ and the protein, first, a charge density study was made on a $NADP^+$ analogue, the NAD^+ cofactor. From this experimental multipolar analysis, the deformation density parameters of $NADP^+$ have been modelled, and then added to the database. The electrostatic potential calculation was therefore performed on a substructure of 64 amino acids (711 atoms) [region highlighted in Fig. 7(b)] surrounding the active site, with and without the $NADP^+$ molecule, using the charge and multipolar parameters of the database. As the inhibitor definition was not available in the database, the system used for the electrostatic potentials computations does not include its contribution.

The electrostatic potential of the free $NADP^+$ cofactor has already been discussed above, and is shown in the active site orientation in Figure 2.

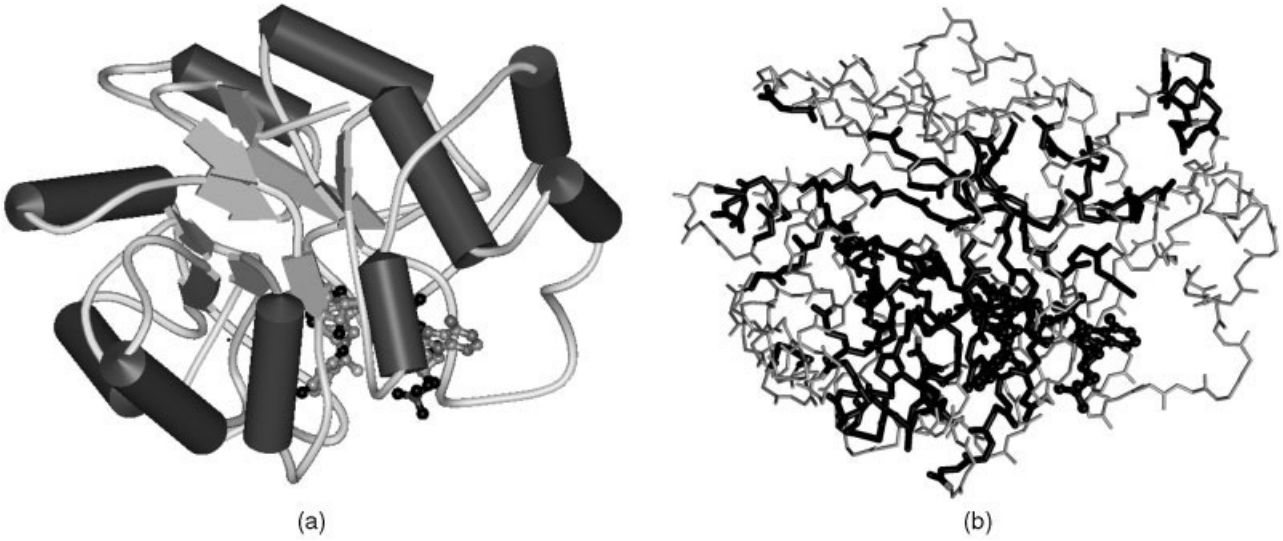

FIGURE 7. (a) Schematic view of the human aldose reductase structure, with alpha helixes represented as tubes, beta strands as arrows, and loops as coils. The $NADP^+$ cofactor and the inhibitor are showed in ball-and-stick mode, indicating the position of the active site. (b) View of the protein C-alpha trace, showed in the same orientation as (a), with the 119 residues of the structure highlighted in bold black where equivalent *B* factors (averaged over non-H atoms) are lower than 4 $Å^2$.

Figure 8(a) gives the electrostatic potential generated by the holoenzyme structure in the active site, plotted in the plane of the $NADP^+$ nicotinamide ring. Figure 8(b) shows the electrostatic potential, in the same orientation as Figures 8(a) and 2, obtained for the apoenzyme, i.e., without the $NADP^+$ con-

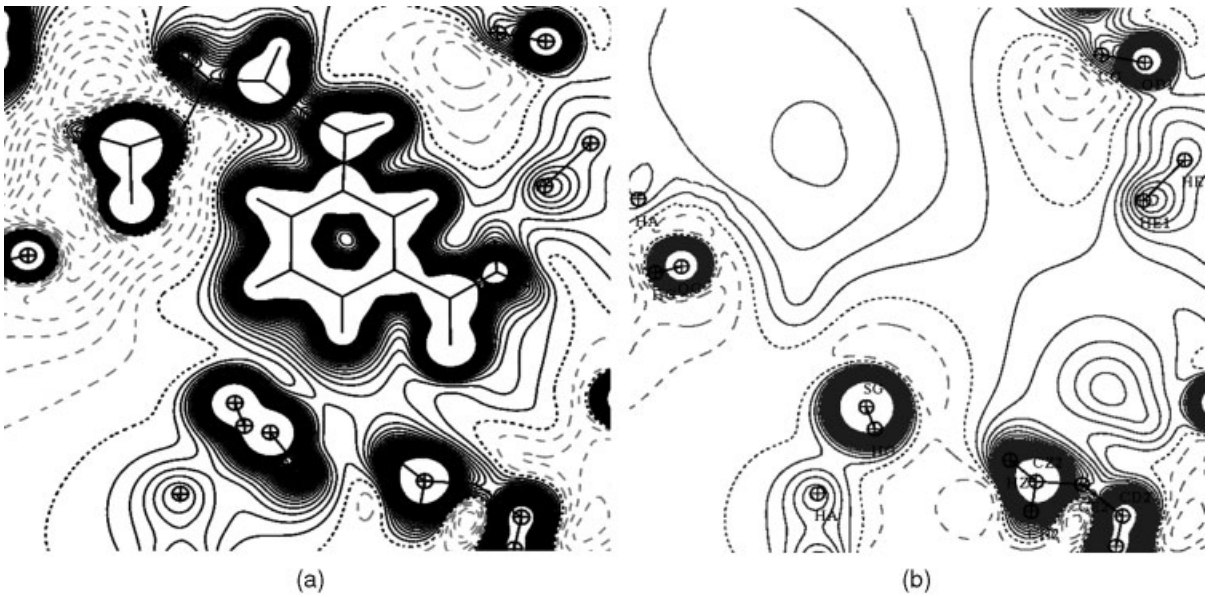

FIGURE 8. (a) Electrostatic potential computed with transferred multipolar parameters as generated by the holoenzyme in the active site, represented in the plane of the $NADP^+$ nicotinamide ring. (b) Electrostatic potential computed without the NADP+ contribution, represented in the same orientation as (a). Contours are 0.05 $eÅ^{-1}$; positive, negative, and zero potentials respectively indicated by full, broken, and dotted lines.

tribution. The apoenzyme electrostatic potential in the binding pocket shows two electropositive regions [top-left and bottom-right in Fig. 8(b)] and two electronegative regions [top-right and bottom-left in Fig. 8(b)]. Comparison between Figures 2 and 8 shows that the electrostatic potential generated by the cofactor alone (in the holoenzyme conformation, Fig. 2), and the one obtained in the apoenzyme active site [Fig. 8(b)] are clearly complementary. For instance, the electronegative potentials generated by the pyrophosphate and the amide oxygen atom of $NADP^+$ are qualitatively complementary to the electropositive potential in the active site, and the same observation can be made for active-site electronegative potentials and $NADP^+$ positive ones. This is all the more remarkable as the $NADP^+$ electrostatic potential has been obtained in a totally independent way: without any assumption related to the active-site geometry or electrostatics. The results of this study were the first experimental charge density demonstration of an electrostatic complementarity between a protein environment and its ligand [4].

Another application has been performed with the allosteric insulin hexamers structure, solved at atomic resolution [34].

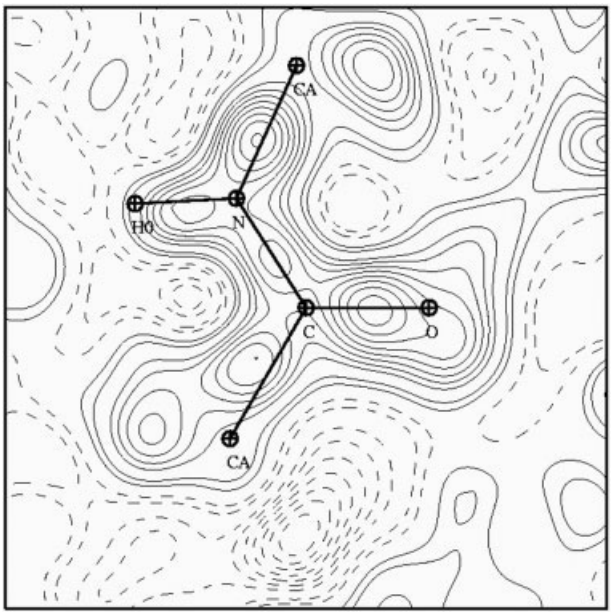

FIGURE 9. Dynamic deformation density on the Tyr47-Cys48 peptide group, computed with transferred multipolar parameters. Contours are 0.02 $eÅ^{-3}$, positive in solid lines, negative in dashed lines.

PROTEIN CHARGE DENSITY REFINEMENT

As previously noted, the subatomic resolution in conjunction with low to moderate atomic thermal motion allows the refinement of the charge density parameters. The starting values for the refinement of the multipolar parameters can be either taken as IAM (neutral valence populations and null multipolar parameters), or as transferred from the multipolar database. We have shown that the latter option leads to more precise charge density description [35].

The first test was performed on the toxin II of the *Androctonus australis* Hector scorpion for which diffraction data at room temperature were collected to d = 0.96 Å resolution [6]. Although the thermal smearing of electron density was higher (average 8 $Å^2$), the procedure described above allowed us to enhance the nonspherical electron density, as shown in Figure 9, where strong electron density peaks are visible on each covalent bonds of the peptide plane. However, the effects of both limited resolution and quite high atomic thermal motion are noticeable around the carbonyl oxygen atom, where no clearly defined accumulation of electron density accounting for the electrons lone pairs are visible.

The second application of the method was the 0.54 Å crambin diffraction data [7] collected at DORIS (Hamburg) by M. Teeter and V. Lamzin. This study has demonstrated the feasibility of the method and was discussed in Part I. The structures of trypsin [36] and of a snake venom phospholipase [37], both at 0.8 Å resolution, were also analyzed recently using the program MoPro; they display clear bonding electron density.

The next application, which is at this time still under way, is the 0.66 Å resolution human aldose reductase, $NADP^+$, inhibitor IDD594 ternary complex. A multipolar refinement of the transferred charge density parameters against the experimental data has been performed. Again, the system effectively used in the refinement was not the full atomic model but only regions of the structure with moderate thermal motion [Fig. 7(b)]. In other words, regions of multiple conformations were avoided, and both the C and N terminus as well as water molecules were not included in the structure subset. The working subset is made of 119 of the 316 amino acids of the enzyme, including the active site residues and the two bonded molecules $NADP^+$ and inhibitor.

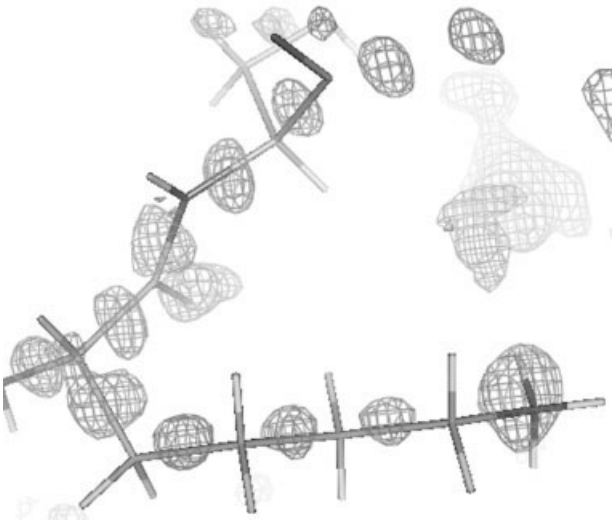

FIGURE 10. Residual electron density in the Lys262 region of the 0.66 Å resolution aldose reductase complex, showing bonding densities along the lysine main and side chains. Contours are 2.4 sigma units.

All the methods described above have been applied: first, an HO refinement of structural parameters has been performed with MoPro [22], for atoms of the structure subset, against successive narrowing high resolution ranges: the first one between 1.0 and 0.66 Å and the last one between 0.75 and 0.66 Å. This method allowed avoiding instabilities in the refinement due to large parameters shifts when the working resolution range goes directly from all the data to the very high resolution only. This HO refinement leads to a significant improvement of the residual densities, which are the expected signal to be modelled by the refinement of the charge density parameters. Strong bonding density peaks are visible in the middle of most of the covalent bonds of the structure subset, as well as around many oxygen atoms, corresponding to the lone pairs. Even in regions usually less ordered in protein structures, such as long amino-acid side chains, the bonding densities are clearly visible, as illustrated in Figure 10 in the case of the Lys262 residue.

The next stage of the procedure consists in the transfer of the database multipolar parameters to the atomic model obtained at the end of the high-order refinement. This transfer lead to an immediate and drastic improvement of the crystallographic agreement factors, with $R(F)$ dropping from 9.28 to 8.79%, and $R_{free}(F)$ from 9.45 to 9.16% (using all the 491.000 experimental data). This means that the procedure allows to take into account most residual density which is the signature of covalent bonding, nonmodeled by the standard spherical refinement using an AIM model. The transferred charge density parameters have then been refined against the full resolution range with the application of symmetry and chemical equivalencies constraints on all moieties. Resulting static deformation densities are represented for the protein peptide plane [Fig. 11(a)] and in the plane of a tyrosine residue side chain [Fig. 11(b)]. A comparison between Figure 11(a) and the peptide group deformation electron density as described in the database (Fig. 3) reveals that no significant deviation occurs for the refined parameters ($<rmsd> = 0.06$ eÅ^{-3}) when the starting values are taken from the database. Actually, this is expected from such a procedure, as this constrained refinement leads to the average protein deformation density, which is close to that described in the database. Figure 11(b) shows the static deformation density in the side-chain plane of a tyrosine residue. The quality of the average charge density in this protein case is comparable to the results one could expect for the electron density on an individual moiety in small-molecule refinement.

Conclusion

We have shown that high-resolution and ultra-high-resolution refinement of proteins is now possible using the multipole model and the new software MoPro. This permits calculation of the electrostatic properties which allows understanding interactions among proteins, ligands, and cofactors. Recent development of diffraction techniques at third-generation synchrotron, as well as progress in cryocrystallography and crystallization, promise more and even higher resolution data sets that will require nonspherical models yielding more accurate structure and protein electrostatics. Electrostatic energy calculations are under way and the resulting energies will be used for example in enzymology to calibrate inhibitors in relation with biochemical activity. A further development of the charge density library will also allow a more quantitative description of the interactions between proteins and nucleic acids. This work should be performed in parallel with theoretical calculations in order to perform comparison of charge density and electrostatic obtained with both methods.

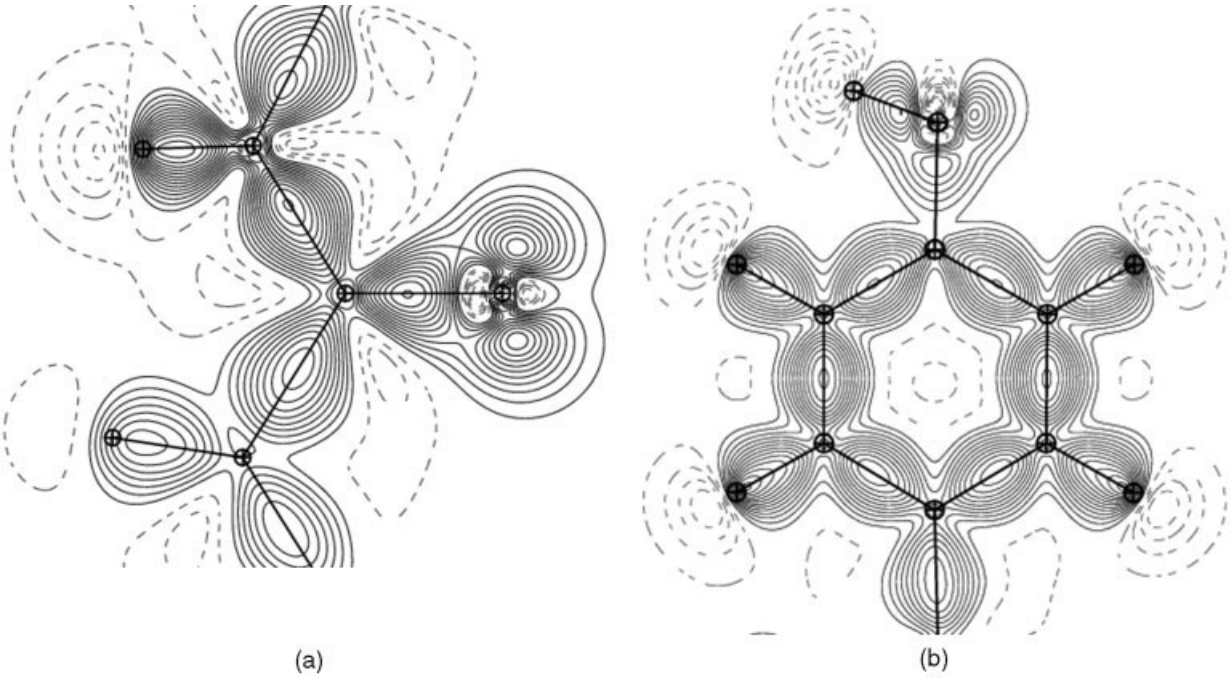

FIGURE 11. Static average deformation densities after a constrained multipolar refinement: (a) in the protein peptide plane; (b) in the C_6 plane of a tyrosine residue. Contours are 0.05 eÅ^{-3}, positive in full and negative in broken lines.

ACKNOWLEDGMENTS

This work was supported by the Centre National de la Recherche Scientifique (CNRS) and by "le Ministère de la Recherche". B. G. thanks the French Ministry of Research and Technology for a PhD fellowship. We thank Drs N. Muzet and V. Pichon-Pesme for fruitful discussions.

References

1. Dauter, Z.; Lamzin, V. S.; Wilson, K. S. Curr Opin Struct Biol 1997, 7, 681–688.
2. Longhi, S.; Czjzek, M.; Cambillau, C. Curr Opin Struct Biol 1998, 8, 730–737.
3. Dauter, Z.; Lamzin, V. S.; Wilson, K. S. Curr Opin Struct Biol 1995, 5, 784–790.
4. Muzet, N.; Guillot, B.; Jelsch, C.; Howard, E.; Lecomte, C. Proc Natl Acad Sci USA 2003, 100, 8742–8747.
5. Schmidt, A.; Jelsch, C.; Rypniewski, W.; Lamzin, V. S. J Biol Chem 2003, 10, 1074.
6. Housset, D.; Benabicha, F.; Pichon-Pesme, V.; Jelsch, C.; Maierhofer, A.; David, S.; Fontecilla-Camps, J. C.; Lecomte, C. Acta Crystallogr, Sect D 2000, 56, 151–160.
7. Jelsch, C.; Teeter, M. M.; Lamzin, V.; Pichon-Pesme, V.; Blessing, R. H.; Lecomte, C. Proc Natl Acad Sci USA 2000, 97, 3171–3176.
8. Stewart, R. F. J Chem Phys 1969, 51, 4569–4577.
9. Hansen, N. K.; Coppens, P. Acta Crystallogr, Sect A 1978, 34, 909–921.
10. Spackman, M. A. Annu Rep Prog Chem C: Phys Chem 1998, 94: 177–207.
11. Bouhmaida, N.; Ghermani, N. E.; Lecomte, C.; Thalal, M. Acta Crystallogr, Sect A 1999, 55, 729–738.
12. Stewart, R. F.; Craven, B. M. Biophys J 1993, 65, 998–1005.
13. Spackman, M. A. J Chem Phys 1986, 85, 6579–6586.
14. Bouhmaida, N.; Ghermani, N. E.; Lecomte, C.; Thalal, M. Acta Crystallogr, Sect A 1997, 53: 556–563.
15. Abramov, Y. A.; Volkov, A.; Wu, G.; Coppens, P. Acta Crystallogr, Sect A 2000, 56: 585–591.
16. Spackman, M. A. Chem Rev 1992, 92: 1769–1797.
17. Soler, J. M.; Artacho, E.; Gale, J. D.; Garcia, A.; Junquera, J.; Ordejon, P.; Sanchez-Portal, D. J Phys Condens Matter 2002, 14, 2745–2779.
18. Fernandez-Serra, M. V.; Junquera, J.; Jelsch, C.; Lecomte, C.; Artacho, E. Solid State Commun 2000, 116, 395–400.
19. Podjarny, A.; Howard, E.; Mitschler, A.; Chevrier, B.; Lecomte, C.; Guillot, B.; Pichon-Pesme, V.; Jelsch, C. Europhys News 2002, 33(4), 113–117.
20. Howard, E.; Cachau, R. E.; Mitschler, A.; Chevrier, B.; Barth, P.; Lamour, V.; Joachimiak, A.; Sanishvili, R.; Van Zandt, M.; Sibley, E.; Moras, D.; Podjarny, A. Structure of monomeric 36kDa human aldose reductase-NADP+-inhibitor complex at 0.66Å resolution; Proteins structure, function and genetics. 2004, in press.

21. Cachau, R.; Howard, E.; Barth, P.; Mitschler, A.; Chevrier, B.; Lamour, V.; Joachimiak, A.; Sanishvili, R.; Van Zandt, M.; Sibley, E.; Moras, D.; Podjarny, A. J Phys (Paris) 2000, 10, 3–13.
22. Guillot, B.; Viry, L.; Guillot, R.; Lecomte, C.; Jelsch, C. J App. Crystallogr 2001, 34, 214–223; J Appl Crystallogr 2004, in press.
23. Souhassou, M.; Lecomte, C.; Ghermani, N. E.; Rohmer, M. M.; Wiest, R.; Bénard, M.; Blessing, R. H. J Am Chem Soc 1992, 114, 2371–2382.
24. Ghermani, N. E.; Lecomte, C.; Bouhmaida, N. Z. Naturforsch, A: Phys Sci 1993, 48, 91–98.
25. Souhassou, M.; Blessing, R. H. J Appl Crystallogr 1999, 32, 210–217.
26. Guillot, B.; Muzet, N.; Artacho, E.; Lecomte, C.; Jelsch, C. J Phys Chem B 2003, 107, 9109–9121.
27. Souhassou, M.; Lecomte, C.; Blessing, R. H.; Aubry, A.; Rohmer, M. M.; Wiest, R.; Bénard, M.; Marraud, M. Acta Crystallogr, Sect B 1991, 47, 253–266.
28. Pichon-Pesme, V.; Lachekar, H. Souhassou, M.; Lecomte, C. Acta Crystallogr, Sect B 2000, 56, 728–737.
29. Pichon-Pesme, V.; Lecomte, C.; Lachekar, H. J Phys Chem 1995, 99, 6242–6250.
30. Jelsch, C.; Pichon-Pesme, V.; Lecomte, C.; Aubry, A. Acta Crystallogr, Sect D 1998, 54, 1306–1318.
31. Lamzin, V. S.; Morris, R. J.; Dauter, Z.; Wilson, K. S.; Teeter, M. M. J Biol Chem 1999, 274, 20753–20755.
32. Sheldrick, G. M.; Schneider, T. S. Methods Enzymol 1997, 276: 319–343.
33. Hirshfeld, F. L. Acta Crystallogr, Sect A 1976, 32, 239–244.
34. Smith, G. D.; Pangborn, W.A.; Blessing, R. H. Acta Crystallogr, Sect D 2003, 59, 474–482.
35. Guillot, B. Extension des méthodes d'affinement multipolaire des petites molécules aux macromolécules. Thèse de l Université Henri Poincaré–Nancy 1, 2002.
36. Schmidt, A.; Jelsch, C.; Rypniewski, W.; Lamzin, V. S. J Biol Chem 2003, 10, 1074.
37. Liu, Q., Teng, Q. H. M.; Weeks, C. M.; Jelsch, C.; Zhang, R.; Niu, L. J Biol Chem 2003, 278, 41400–41408.